Cavity Ringdown Spectroscopy of the $\tilde{A} - \tilde{X}$ Electronic Transition of the $CH_3C(O)O_2$ Radical

Sergey J. Zalyubovsky, Brent G. Glover, and Terry A. Miller*

Laser Spectroscopy Facility, Department of Chemistry, The Ohio State University, 120 W. 18th Avenue, Columbus, Ohio 43210

Received: April 28, 2003; In Final Form: July 14, 2003

Cavity ringdown spectra of the near-IR $\tilde{A}^2A' - \tilde{X}^2A''$ electronic transition of the acetyl peroxy radical and its perdeutero analogue are reported. The electronic origin for the $CH_3C(O)O_2$ is observed at 5582.5(5) cm^{-1}. Extensive ab initio calculations have been carried out to predict frequencies and help assign the electronic origin, observed vibrational hot bands, and several $\tilde{A}$ state vibrational frequencies. An empirical absorption cross section for the origin of the $\tilde{A}^2A' - \tilde{X}^2A''$ transition is estimated at $\sigma_{CH_3C(O)O_2} = (1\pm0.5) \times 10^{-19}$ cm^2.

1. Introduction

The acetyl peroxy $CH_3C(O)O_2$ radical is one of the most abundant and important organic peroxy radicals in the atmosphere.[1] Atmospheric oxidation or upper tropospheric photolysis of a variety of oxygen containing organic compounds, acetone, acetaldehyde, methyl glyoxal, etc., can lead to the formation[2,3] of the acetyl peroxy radical, $CH_3C(O)O_2$. This radical, as well as other peroxy radicals, plays a significant role in many key atmospheric processes.[4,5] It can affect ozone destruction in the stratosphere by linking odd O cycles. Peroxy radical participation in tropospheric NO_x cycles is considered to be a major source of tropospheric ozone production. The acetyl peroxy reaction with HO_2 is believed to be responsible for acid rain formation and can also lead to the production of ozone and atomic oxygen.[6,7] Fast acetyl peroxy self-reaction results in the generation of methyl peroxy radical,[8,9] another very important intermediate in atmospheric chemistry.

Acetyl peroxy radicals are of particular importance in polluted atmospheres as they react with NO_2 and form peroxy acetyl nitrate (PAN). PAN has been identified as a key component in photochemically generated smog.[10] It can irritate eyes and damage crops.[11,12] PAN has a relatively high stability to thermal decomposition compared to other peroxy nitrates,[13] and therefore, it can serve as an efficient reservoir for both $CH_3C(O)O_2$ and NO_2. PAN can be transported from sources of pollution to remote locations or to the upper troposphere where it decomposes photolytically,[14] to regenerate the reactive radicals.

Similar to the other members of the peroxy family, the vast majority of the spectroscopic and kinetic research on the acetyl peroxy radical has been performed using its UV $\tilde{B}^2A'' - \tilde{X}^2A''$ electronic transition.[15] This transition is broad and structureless because of the repulsive nature of the $\tilde{B}$ state, which makes it inapplicable for rotational or vibrational spectroscopic analysis. Despite its large absorption cross sections ($\sim10^{-18}$ cm^2), kinetic experiments of a mixture of peroxy radicals become compromised because nearly all peroxy radicals have nearly superimposable $\tilde{B}-\tilde{X}$ UV bands.[16]

The infrared $\tilde{A}^2A'-\tilde{X}^2A''$ transition has been viewed as an ideal candidate to overcome the aforementioned difficulties. It has been observed for several peroxy radicals in early low resolution modulated absorption experiments[17] and intracavity laser absorption studies.[18] It has a relatively small ($\sigma \approx 10^{-21}-10^{-20}$ cm^2) transition[19,20] moment, but the cavity ringdown spectroscopy (CRDS) technique has evolved into a powerful tool for spectroscopic observations of weakly absorbing transient species.[21,22] Our group has reported application of the CRDS technique to study the $\tilde{A}^2A' - \tilde{X}^2A''$ transition of peroxy radicals, and sharp, structured spectra for several alkyl peroxy and fluorinated methyl peroxy radicals have been reported.[20,23] Recently, a CW version of CRDS has been applied to study alkyl peroxy radical spectroscopy and kinetics.[24]

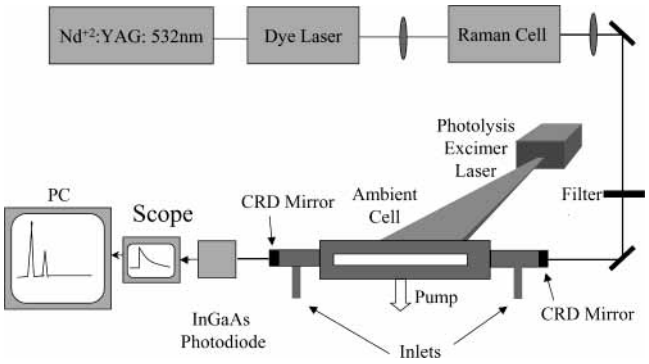

Figure 1. Near-IR cavity ringdown apparatus.

In this paper, we report observation of $\tilde{A}^2A'-\tilde{X}^2A''$ transition of acetyl peroxy radical using our IR extended CRDS apparatus. A recently suggested source of chlorine atoms is implemented in the acetyl peroxy production scheme. To facilitate spectroscopic assignment, ab initio calculations for the $\tilde{A}$ and $\tilde{X}$ states of the cis and trans conformers of acetyl peroxy radical have been carried out to predict geometry, vibrational frequencies and the transition frequency T_{00} for the electronic origin.

2. Experimental Section

2.1. Near-IR Cavity Ringdown Apparatus. A diagram of the experimental apparatus used in our experiments is shown in Figure 1. Light generated by a Nd:YAG pumped dye laser system (20 Hz PRO-270 Nd:YAG, Spectra Physics and PDL-2 Dye laser, Quanta Ray) was shifted into the near-infrared region via stimulated Raman scattering in molecular hydrogen. Operat-

* To whom correspondence should be addressed.

10.1021/jp0305279 CCC: $25.00
Published on Web 08/26/2003

ing with the set of LDS765, LDS750, LDS721, LDS698, and DCM laser dyes (Exiton), this system was tuned over the 775−670 nm region with pulse energies of 30−40 mJ and 0.3 cm^{-1} (fwhm) laser line width. A 50 cm focal length lens was used to focus the laser beam into the middle of the 70 cm long single pass Raman cell pressurized with 300−400 psi of H_2. Output radiation was spectrally filtered using several 1.3 or 1.4 μm cutoff longwave pass filters (CVI, Spectrogon) to eliminate anti-Stokes, fundamental, and first Stokes radiation. The resulting 1−2 mJ of second Stokes radiation in the 2.17−1.51 μm region was delivered to the ringdown cell through two 1m focal length lenses to approximate a TEM_{00} cavity mode.

The ringdown cavity was formed by two 6 m curvature plano-concave mirrors (Los Gatos Research) separated by 55 cm to ensure a stable resonator configuration. Mirrors were attached to the arms of a stainless steel cell using fine adjustment mounts. The cell was manufactured with various ports for precursor gas inlets, purges, pressure gauge (Baratron), and exhaust for a mechanical vacuum pump. The ringdown mirrors were constantly purged during the course of experiments with a positive nitrogen flow to protect the mirror surfaces from any harsh chemical environment present in the cell. Two rectangular (2 × 18 cm) apertures separated by 2.3 cm were made in the center of the cell for UV grade quartz photolysis windows. The radiation leaving the ringdown cavity was focused by a 2.5 cm focal length lens on an amplified photodiode. A ThorLabs InGaAs (PDA 255) or Judson Technologies InAs (J12) photodiode was used depending on the spectral range of operation. The detector output was recorded by a 12 bit 20 MS/s digitizing card (Measurement Computing) for further analysis. Typically, 20 laser shots per frequency point were averaged. The transient decay was fitted to a single exponential for decay time, initial amplitude and baseline using the nonlinear Levenberg−Marquardt algorithm. The decay constant was converted to the cavity absorption per pass (in ppm) and saved as a point in the spectrum. During experiments regular checks were performed to reveal any systematic errors by analyzing a noise histogram for normal distribution. Typical empty cavity baseline absorption was 53.5 ppm with standard deviation of 0.3 ppm and fractional error of ~0.6% which is typical for pulsed ringdown applications.[25]

The photolysis excimer laser (LPX300, Lambda Physik) was operated at 193 nm, and the beam was shaped by cylindrical and spherical lenses to a rectangle 13×0.5 cm and sent through the photolysis windows into the central part of the flow cell. Background absorption of the precursors and residual water vapor were eliminated by subtraction of data points taken with the excimer laser on and off for each laser step. All data was calibrated with 0.25 cm^{-1} accuracy using H_2O and HCl overtones with the frequencies taken from HITRAN[26] database. Control of the lasers, fitting procedure, and experimental time sequence were performed by a PC-based Labview data acquisition software.

2.2. Acetyl Peroxy Production and Kinetics. Photolysis of $(COCl)_2$ in $CH_3CHO/O_2/N_2$ mixture has been used to produce acetyl peroxy radicals. The reaction mechanism is likely

$$(COCl)_2 \xrightarrow{193\ nm} 2Cl + 2CO \quad (1)$$

$$CH_3CHO + Cl \rightarrow CH_3CO + HCl \quad (2)$$

$$CH_3CO + O_2 + N_2 \rightarrow CH_3C(O)O_2 + N_2 \quad (3)$$

Recently photolysis of oxalyl chloride $(COCl)_2$ has been proposed[27] as a clean source of Cl atoms. It has a large ($\sigma_{OxCl} = 3.8 \times 10^{-18}$ cm^2) absorption cross section at 193 nm, and only Cl and CO have been reported[28,27] as dissociation products in reaction 1. Carbonylic hydrogen abstraction in reaction 2 has been shown as a predominant (93%) channel in experimental observations[29] supported by theoretical considerations,[30] and therefore, formation of the methyl formyl radical in this reaction is neglected in our kinetic mechanism. Acetyl peroxy formation via reaction 3 is followed by radical recombination reactions.

TABLE 1: Kinetic Mechanism for the Acetyl Peroxy Radical Formation

reaction	k (298 K) cm^{-3}/molecule s	ref
$CH_3CHO + Cl \rightarrow CH_3C(O) + HCl$	7.8×10^{-11}	36
$CH_3C(O) + CH_3C(O) \rightarrow$ products	7.47×10^{-11}	37
$CH_3C(O) + O_2 + N_2 \rightarrow CH_3C(O)O_2 + N_2$	5×10^{-12}	38
$CH_3C(O)O_2 + CH_3C(O)O_2 \rightarrow 2CH_3 + 2CO + 2O_2$	1.64×10^{-11}	38
$CH_3 + O_2 + N_2 \rightarrow CH_3O_2 + N_2$	2.9×10^{-12}	39
$CH_3C(O)O_2 + CH_3O_2 \rightarrow$ products	1.26×10^{-11}	38
$CH_3C(O)O_2 + Cl \rightarrow$ products	1.6×10^{-10}	39[a]
$CH_3C(O) + Cl \rightarrow CH_2CO + HCl$	1.79×10^{-10}	40
$Cl + O_2 \rightarrow$ products	1.7×10^{-14}	39

[a] Rate constant for the chlorine atom reaction with acetyl peroxy radical is assumed to be the same as for the $CH_3O_2 + Cl$ reaction.

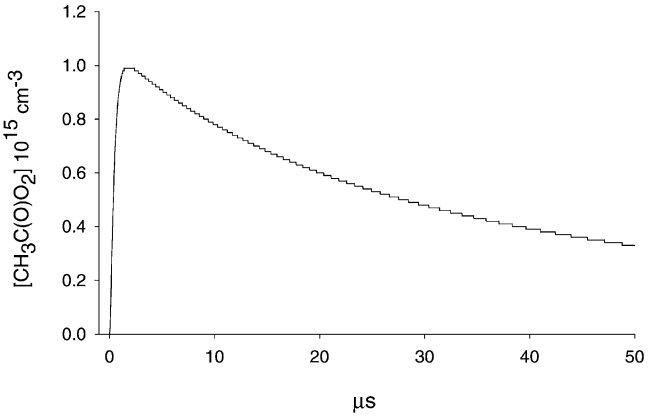

Figure 2. Simulation of the acetyl peroxy temporal profile using the reaction mechanism provided in Table 1 and initial concentrations listed in the text. Because of excess concentrations of CH_3CHO and O_2, chlorine atoms are stoichiometrically converted to $CH_3C(O)O_2$.

Typical concentrations of the reactants in our experiments (in Torr) are $[(COCl)_2] = 0.5$, $[CH_3CHO] = 1$, $[O_2] = 50$, $[N_2] = 150$. With the $\sim 9 \times 10^{15} cm^{-2}$ flux of 193 nm photons, about seven percent of the $(COCl)_2$ molecules will be dissociated yielding 1×10^{15} cm^{-3} of Cl atoms. Using the set of reactions and rate constants presented in Table 1 and the above initial concentrations for the reactants, one can simulate acetyl peroxy radicals evolution under ambient cell conditions. Figure 2 shows that within several microseconds after photolysis pulse, effectively all Cl atoms will be consumed by acetaldehyde and $\sim 1 \times 10^{15}$ cm^{-3} acetyl peroxy radicals will be formed. In some experiments, 193 nm photolysis of biacetyl $(CH_3CO)_2$ was used as alternative source of acetyl radical to support spectroscopic assignment of the spectral carrier.

Direct photodissociation[3] of CH_3CHO in the presence of oxygen may introduce other reactive species (HCO, HO_2, and CH_3O_2) into the system, but all four components—193 nm excimer light, oxalyl chloride, acetaldehyde, and oxygen—are necessary to observe the spectroscopic transitions described below. Additionally, because of the small ($\sim 10^{-21}$ cm^2) acetaldehyde UV absorption cross section[31] only $\sim 10^{12}$ cm^{-3}

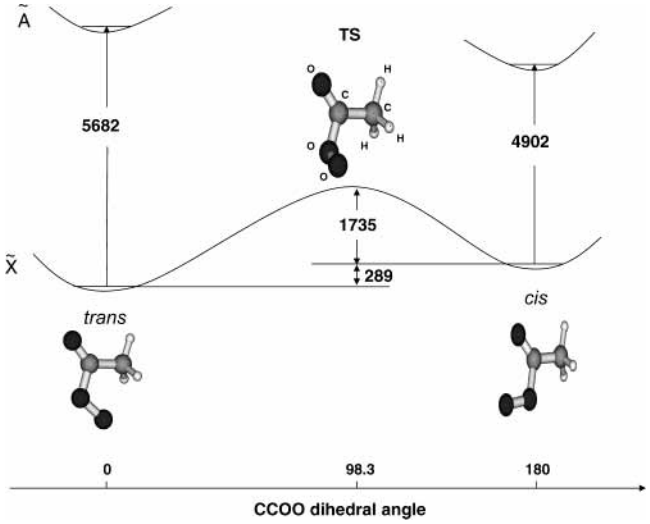

Figure 3. Results of the G2 calculations for the origin of the $\tilde{A}-\tilde{X}$ electronic transition and the barrier between trans and cis acetyl peroxy radicals in cm^{-1}. Trans acetyl peroxy conformer is slightly lower in energy, probably because of a slight bonding interaction between the oxygen and the methyl hydrogens.

TABLE 2: G2 Calculations and Experimental Values (in cm^{-1}) for the Electronic Origins of $\tilde{A}-\tilde{X}$ Transitions of Various Peroxy Radicals[a]

T_{00}	HO_2	CH_3O_2	$C_2H_5O_2$	i-$C_3H_7O_2$	CF_3O_2
ab initio	7061	7375	7355	7771	6703
expt	7041(2)[17]	7382.8(5)[20]	7590(3)[20]	7568(3)[41]	6656(3)[23]
expt−ab initio	−20	7	235	−203	−47

[a] The standard error for G2 energy calculations[34] is 350 cm^{-1}.

acetaldehyde photofragments can be produced in our system, which would be negligible compare to the considered kinetic mechanism.

The subsequent fate of the acetyl peroxy radicals is primarily guided by self-reaction and reaction with other peroxy radicals (see Table 1). Because of the precursors, the typical background absorption baseline is around 200−300 ppm which corresponds to ~7 μs ringdown time for our experimental setup. As Figure 2 shows, assuming initial concentration of 1×10^{15} cm^{-3} and putative second-order decay, the half-life of the acetyl peroxy radicals in the cell is 28 μs, which is long enough compared to the ringdown decays. In practice typical concentrations are factor 1.5−2 smaller with a corresponding increase in lifetime.

Under our experimental conditions, the rate of the radical axial diffusion losses is estimated to be a negligible 2.5 s^{-1}. The excimer laser is fired 5 μs before the probe laser, allowing sufficient time for peroxy formation.

Concentrations of the reactants were controlled by calibrated mass flow controllers (MKS). Additionally, the $(COCl)_2$ concentration was monitored by its UV absorption at 193 nm. Pump speed was set to 100 cm^3/s. With a photolysis volume of 15 cm^3 and laser system repetition rate of 20 Hz, the photolysis mixture is replaced every third laser pulse. 4.3 UHP grade O_2 and N_2 (5.0 research grade) were used. Oxalyl chloride (99%), aldehyde (99.5%), *d4*-aldehyde(98%), and biacetyl (99%) were obtained from Aldrich. Liquid compounds were purified by repeated freeze−pump−thaw cycles at 77 K and premixed in N_2 with the following concentrations: 0.5% $(COCl)_2$, 10% CH_3CHO or CD_3CDO.

3. Results and Discussion

3.1. Ab Initio Calculations. To support and predict our spectroscopic observations, we have performed ab initio calculations on the acetyl peroxy radical and its perdeutero analogue using the Gaussian 98 package. The acetyl peroxy radical, similar to other $RC(O)O_2$ peroxy radicals,[32,33] can exist in cis and trans stable conformational forms, interconverted by O−O internal rotation around the C−O bond. C_s symmetry for the ground (A'') and exited (A') state minima geometry for both conformers was first found using low level UHF calculations. Then, the excitation frequency for the $\tilde{A}^2A'-\tilde{X}^2A''$ electronic transition and the relative energy for both conformers were calculated using the G2 method. The barrier to the O−O internal rotation was calculated at the G2 level following transition state geometry optimization. Results of the G2 calculations, geometries for cis and trans acetyl conformers of peroxy, as well as the transition state are shown in Figure 3. Frequencies for the $\tilde{A}-\tilde{X}$ transitions were obtained using the zero-point corrected electronic energy (G2(0 K)) outputed by the program.

To check the accuracy of G2 method, we have performed G2 calculations for numerous peroxy radicals, and the results are present in Table 2. Maximum disagreement between experimental observations[17,20,23] and theoretical predications is around 250 cm^{-1}, which is well within the error bars reported for the G2 method.[34]

In the spectrum, one should expect transitions to the origin and exited vibrational levels of the $\tilde{A}$ state from the vibrationless level of the $\tilde{X}$ state. One should also expect to observe hot bands

TABLE 3: Scaled (0.89) UHF/6-31+G(d) Frequencies of Several Low Lying Vibrations in the trans and cis Acetyl Peroxy Radicals and Their Perdeutero Analogues[a]

	$\tilde{A}$	$\tilde{X}$	$\Delta(\nu_{\tilde{A}} - \nu_{\tilde{X}})$	expt	mode	symmetry	$\exp(-\nu_{\tilde{X}}/kT)$
	144	126	18	43(1)	C(O)O wag	A″	0.54
trans-$CH_3C(O)O_2$	163	182	−19	−13(1)	CH_3 torsion	A″	0.41
	286	320	−34	−44(1)	CCO bend	A′	0.21
	116	121	−5	−6(1)	CD_3 torsion	A″	0.56
trans-$CD_3C(O)O_2$	143	135	8	39(1)	C(O)O wag	A″	0.52
	266	295	−29	−43(1)	CCO bend	A′	0.24
	58	93	−35	−13(1)	CH_3 torsion	A″	0.64
cis-$CH_3C(O)O_2$	186	143	43	43(1)	C(O)O wag	A″	0.50
	265	301	−36	−44(1)	CCO bend	A′	0.23
	42	57	−15	−6(1)	CD_3 torsion	A″	0.76
cis-$CD_3C(O)O_2$	178	137	41	39(1)	C(O)O wag	A″	0.51
	255	282	−27	−43(1)	CCO bend	A′	0.25

[a] Experimental values are obtained by measuring separation between 0_0^0 band and the first member of the hot band progression according to the assignment in Figure 4. At room-temperature, all of the listed vibrational levels will have a population comparable to that of the vibrationless levels and transitions originating from those levels should have intensities similar to the origin transition. The next vibrational frequency for both conformers is ≈500 cm^{-1} with a corresponding level population of 0.1 relative to the vibrationless level, and therefore, higher frequency levels were not considered in the hot band analysis.

TABLE 4: Ab Initio B3LYP/6+31-G(d) Rotational Constants for cis and trans $CH(D)_3C(O)O_2$ in GHz

	$CH_3C(O)O_2$			$CD_3C(O)O_2$		
trans	A	B	C	A	B	C
$\tilde{A}$	9.4500	4.68775	3.1960	7.8186	4.5331	2.9762
$\tilde{X}$	9.2073	4.78426	3.2107	7.6489	4.6110	2.9827
cis	A	B	C	A	B	C
$\tilde{A}$	10.4206	4.3173	3.1120	9.4815	3.8440	2.8320
$\tilde{X}$	10.3699	4.3789	3.1389	9.4436	3.8934	2.8547

originating from low lying vibrations in the ground-state populated at room temperature. To predict vibrational features in the spectrum, frequency calculations have been done using the UHF/6-31+G(d) method for $\tilde{A}$ and $\tilde{X}$ states for both acetyl peroxy conformers and their per-deutero analogues. Frequencies for several low lying vibrational modes are listed in Table 3. Geometry optimization for both acetyl peroxy conformers and their perdeutero analogues on B3LYP/6-31+G(d) level has yielded the rotational constants shown in Table 4.

3.2. Spectral Observations and Analysis. The key issue to be confronted is whether the carrier of these spectra is the acetylperoxy radical and, if so, whether it is the cis or trans conformer. Certainly as documented in section 2.2, the chemistry is expected to produce $CH_3C(O)O_2$ in relative abundance, and this is one of the most persuasive arguments as to the spectral carrier. However, such arguments can never rule out all possible minor channels or be totally conclusive.

Further evidence for $CH_3C(O)O_2$ can be derived from the spectrum itself. The only likely transitions for small organic molecules under these conditions in this spectral region are between a ground electronic state and a low-lying one or a vibrational overtone or combination band in the ground state. Considering the chemistry involved, the only likely species present with a NIR electronic transition are peroxy radicals. Peroxy radicals other than acetyl peroxy will have transitions in this frequency region, but the chemistry seems overwhelmingly to favor acetyl peroxy radical.

Vibrational overtones or combinations are expected to be quite weak and are likely at or below the level of detectivity. The strongest such transitions likely involve at least one, and more likely two quanta of CH stretch. As we see below, the observed isotope shifts do not support this hypothesis.

Experimental CRDS spectral traces are shown in Figure 4, traces A and B, respectively, using acetaldehyde or *d4*-acetaldehyde as precursors. The position of the strongest band on trace A of Figure 4 centered at 5582.5(5) cm^{-1} is in a good agreement with both the predicted ab initio T_{00} value for the trans acetyl peroxy conformer given in Figure 3 and the acetyl peroxy origin assignment (5562(3) cm^{-1}) based on previous low resolution experiments.[17] The strongest band in trace B is positioned at 5589.6(5) cm^{-1}.

The observed blue shift of 7 cm^{-1} is consistent with the first-order effect of deuteration on the electronic origin because of a change in the zero-point energy level. Based upon the ab initio

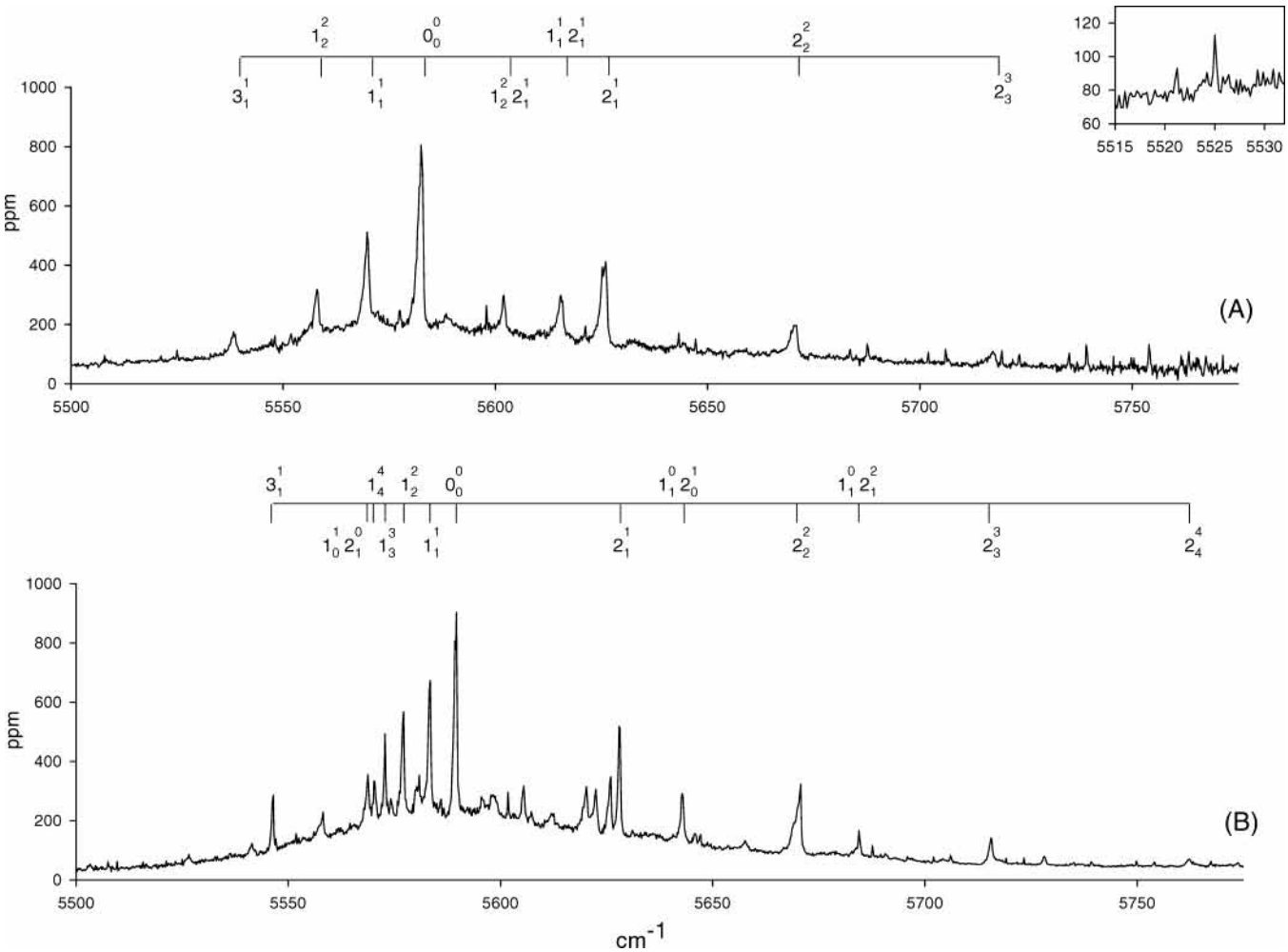

Figure 4. CRDS spectra of the origin of the $\tilde{A}^2A'-\tilde{X}^2A''$ electronic transition of the acetyl peroxy radical taken with CH_3CHO (trace A) and CD_3CDO (trace B) as precursors. Hot bands are labeled according $N_{v''}^{v'}$ notation. Vibration ν_1 is a methyl torsion, ν_2 is a COO wag, and ν_3 ia a CCO bend. The insert shows two P(6) lines from the $H^{37}Cl$ and $H^{35}Cl$ first overtone bands left after background subtraction procedure.

TABLE 5: Observed Origin Frequencies, Hot Band Positions, and Their Relative Shifts with Respect to the Origin for $CH_3C(O)O_2$ and $CD_3C(O)O_2$[a]

cm^{-1}	assignment	position	$\Delta(\nu_{hotband} - 0_0^0)$
	0_0^0	5582.5	0
	1_1^1	5569.8	−12.7
	1_2^2	5558.0	−24.5
	2_1^1	5625.7	43.2
$CH_3C(O)O_2$	2_2^2	5670.5	88.0
	2_3^3	5717.2	134.7
	3_1^1	5538.5	−44.0
	$1_1^1 2_1^1$	5615.5	33.0
	$1_2^2 2_1^1$	5601.9	19.4
	0_0^0	5589.6	0
	1_1^1	5583.4	−6.2
	1_2^2	5577.1	−12.5
	1_3^3	5572.8	−16.8
	1_4^4	5570.3	−19.3
	2_1^1	5628.1	38.5
$CD_3C(O)O_2$	2_2^2	5670.0	80.4
	2_3^3	5715.6	126.0
	2_4^4	5762.2	172.6
	3_1^1	5546.4	−43.2
	$1_0^1 2_1^0$	5568.6	−21
	$1_1^0 2_0^1$	5642.8	53.2
	$1_1^0 2_1^2$	5684.4	94.8

[a] Vibrational hot bands are labeled according to $N_{\nu''}^{\nu'}$ notation, where ν'' and ν' are $\tilde{X}$ and $\tilde{A}$ vibrational quantum numbers in vibration N. Vibration ν_1 is a methyl torsion, ν_2 is a C(O)O wag, and ν_3 is a CCO bend. Each peak position is measured within ± 0.5 cm^{-1}, but because of differing rotational contours, the precision of the resulting vibrational frequencies is somewhat less.

calculations, the difference between $\tilde{A}$ and $\tilde{X}$ zero-point energies for protonated and deuterated trans acetyl peroxy is −112 and −104 cm^{-1}, respectively, meaning that the origin transition for deuterated trans acetyl peroxy should be shifted to the blue by roughly 8 cm^{-1} with respect to the protonated origin. For the cis conformer, the same considerations predict a slightly smaller 2 cm^{-1} blue shift for the deuterated origin. The effect of deuteration on species with CH stretching vibrations with possible overtones residing in this region would have been significantly more pronounced. For instance, in trans acetyl peroxy, the calculated frequency for the symmetric CH stretch will decrease from 2979 to 2212 cm^{-1} upon deuteration, leading to an ≈1500 cm^{-1} red shift upon deuteration.

Results from ab initio calculations for the frequencies of the low lying vibrational modes of the $\tilde{X}$ and $\tilde{A}$ states are given in Table 3. The general appearance of the spectrum can be explained by the presence of vibrational hot bands. Transitions from thermally populated vibrational levels in the $\tilde{X}$ state to the vibrational levels of the same symmetry in the $\tilde{A}$ state are allowed. With respect to the $\tilde{X}$ state, excitation to the $\tilde{A}$ state in both cis and trans conformers will result in a decrease of the CH_3 torsional and an increase of the $C(O)O_2$ wag vibrational frequencies. Therefore, red-shifted torsional and blue-shifted wag hot band progressions are expected in the spectrum.

Based on the aforementioned ab initio considerations, we have assigned several members of the methyl torsion (ν_1), COO wag (ν_2), and CCO bend (ν_3) hot band progressions. Additionally, several hot bands originating from ν_1 and ν_2 combination levels are assigned as well. Positions of the individual hot bands and shifts, relative to the origin, for $CH_3C(O)O_2$ are presented in Table 5 and depicted in Figure 4, trace A.

Referring to Table 5, we note red shifted progressions of −12 and −44 cm^{-1} (single line) spacing. Table 3 has comparable ab initio predictions, which due to the fact that we are computing differences in vibrational frequencies are semiquantitative at best. Nonetheless, we see from Table 3 that the CH_3 torsion and CCO bend hot bands should be shifted with respect to the origin by −19 and −34 cm^{-1} for the trans isomer and −35 and −36 cm^{-1} for cis isomer. Thus, in Table 5, we assign the two red shifted vibrations to ν_1 (CH_3 torsion) and ν_3 (CCO bend). In Table 5 there is a blue shifted progression with spacing ≈44 cm^{-1}, which correlates well with the blue shift predicted for ν_2 (COO wag) of +18 cm^{-1}(trans) or 43 cm^{-1}(cis). Assignment of ν_1 and ν_3 further allows a couple of combination bands to be assigned as shown in Figure 4 and Table 5.

Ab initio calculations can also aid in finding ν_1, ν_2, and ν_3 counterparts in the deuterated spectrum. As Table 3 shows, upon deuteration, the methyl torsional frequency drops which manifests itself in the experimental spectrum of $CD_3C(O)O_2$ shown in Figure 4, trace B, as smaller separations (see Table 5) between members of the torsional (ν_1) hot band progression. Conversely, Table 3 shows that the $C(O)O_2$ wag and CCO bend modes are almost unaffected by deuteration, leaving the separations in the ν_2 and ν_3 hot band progressions almost unchanged. Assignments and frequencies for the $CD_3C(O)O_2$ hot bands are listed in Table 5.

Some of the combination hot bands in the deuterated spectrum do not have obvious correlations in the protonated one. The two low-frequency vibrations listed in Table 3 are A″ symmetry. For an $\tilde{A}^2A'-\tilde{X}^2A''$ electronic transition, all vibronic transitions between modes with the same symmetry are allowed given favorable Franck−Condon factors. In the case of the deuterated acetyl peroxy, especially in the trans conformer, the CD_3 torsion and $C(O)O_2$ wag are almost degenerate. This may result in various effects, such as vibrational resonances, intensity borrowing, enhanced combination bands, etc. leading to a spectrum enriched in hot band combinations.

The individual peaks in Figure 4 correspond to the rotational contours of vibronic transitions. Such rotational contours might allow us to distinguish between cis and trans conformers. Room-temperature simulations of the rotational contour for $\tilde{A}^2A'-\tilde{X}^2A''$ transition with ab initio rotational constants (Table 4) at our experimental resolution have revealed similar overall rotational contours for both trans and cis acetyl peroxy conformers as shown in Figure 5. However, some features in the trans conformer simulations are in better agreement with experimental observations. A strong unresolved Q branch in the trans simulated rotational contour has a width similar to the width of individual peaks in the observed spectra. Deuteration of the trans conformer will result in a rotational contour with a somewhat sharper Q branch, which is consistent with our experimental observations. Rotational simulations for the cis conformer predict a broader than experimentally observed Q branch and also show that the shape of the Q branch is almost unaffected by deuteration, contrary to the experimental observations. Convolution of individual rotational contours of the origin band and multiple vibrational hot bands gives rise to the spectra shown in Figure 4.

All previously observed RO_2 peroxy radicals have a strong OO stretching vibrational progression in the $\tilde{A}$ state because of the unpaired electron on the terminal oxygen. Typical frequencies for this vibration fall around 920 cm^{-1} depending on the nature of the R group.[17,23] In our search for $\tilde{A}$ state vibrational bands of protonated acetyl peroxy, we have covered the region between 5470 and 6650 cm^{-1} (with a small gap between 5790

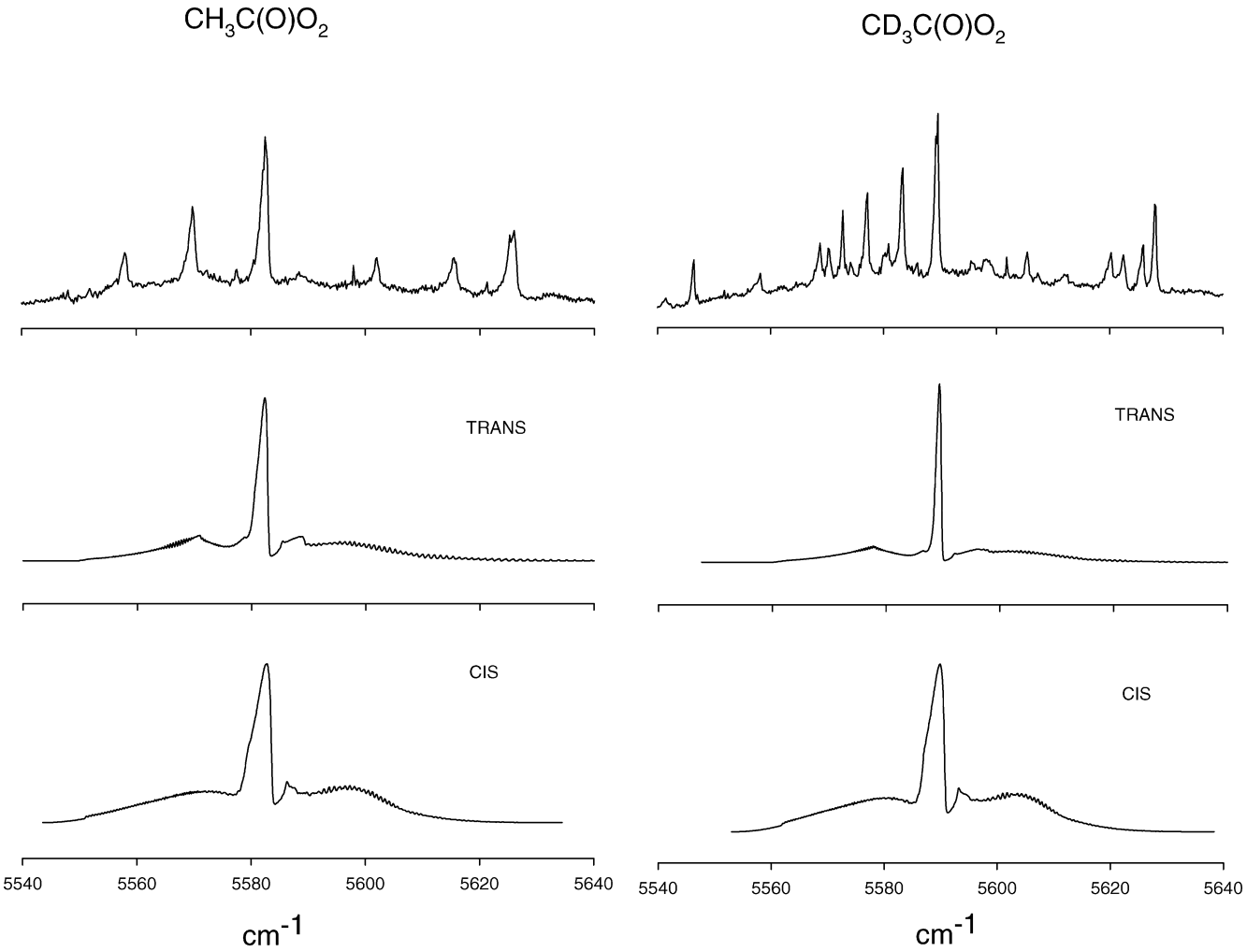

Figure 5. Comparison between observed and simulated rotational contours of the trans and cis acetyl peroxy radicals and their perdeutero analogues. Room-temperature rotational contours are simulated using our SpecView[42] spectral analysis program and ab initio rotational constants from Table 4.

and 5890^{-1} due to insufficient overlap of ringdown mirrors). All bands observed in this region are presented in Figure 6. The close resemblance of the bands in Figure 6 allows us to attribute them to the same molecular species. The strongest peak in trace c of Figure 6 is positioned at 6511(1) cm^{-1} and separated from the origin, trace a, by 929(1) cm^{-1}, which is in excellent agreement with the OO stretching frequency observed for other peroxy radicals.

Further confirmation is obtained by observing the COO bending vibration specific for acetyl peroxy[17] and presented in trace b. This band has its strongest peak at 6121(1) cm^{-1} shifted 539(1) cm^{-1} to the blue from the origin. An additional band has been observed at 6055(1) cm^{-1}, shifted 473(1) cm^{-1} to the blue from the origin and assigned to a CCOO backbone vibration based on the ab initio calculations provided in Table 6. The frequencies of the observed $\tilde{A}$ state vibrations are in a good agreement with ab initio calculations especially for the trans acetyl peroxy conformer.

To confirm the chemical identity of the spectral carrier, some experiments have been carried out with an alternative production scheme. Similar spectral features, but with considerably less signal-to-noise, have been observed when direct photolysis of biacetyl was used to produce the acetyl radical.

Based on the totality of the observed spectroscopic data, analysis and ab initio calculations, the observed spectrum is very likely the $\tilde{A}^2A'-\tilde{X}^2A''$ electronic transition of $CH_3C(O)O_2$, with an origin at 5582.5(5) cm^{-1} and the other bands represent transitions to the exited $\tilde{A}$ state and vibrational hot bands. Although not as certain, based particularly on the agreement of the observed and predicted band origin, shape of the rotational contour, and agreement between predicted and observed vibrational frequencies for the $\tilde{A}$ state, it is most likely that the observed spectrum is due to the trans acetyl peroxy conformer.

We have searched in the region of 4600−5200 cm^{-1} where the cis conformer origin is predicted by G2 calculations and no spectra attributable to the cis acetyl peroxy radical have been observed. The cis conformer is predicted to be higher in energy than the trans one by 290 cm^{-1}, and at room-temperature, its equilibrium population is therefore decreased by a factor of 4 compared to that of the trans conformer. If the calculated energy difference is underestimated (increasing the separation between cis and trans conformer by a factor of 2 gives a factor of 18 in their relative population) and/or the cis absorption cross section is less favorable than the trans one, the cis absorption signal might well fall below our sensitivity. Alternatively, the G2 prediction might be unusually inaccurate in the specific case of the cis acetyl peroxy radical, and its origin may simply reside outside the searched spectral region. Future high resolution rotational studies of the observed bands are necessary to unambiguously distinguish between cis and trans acetyl peroxy conformers.

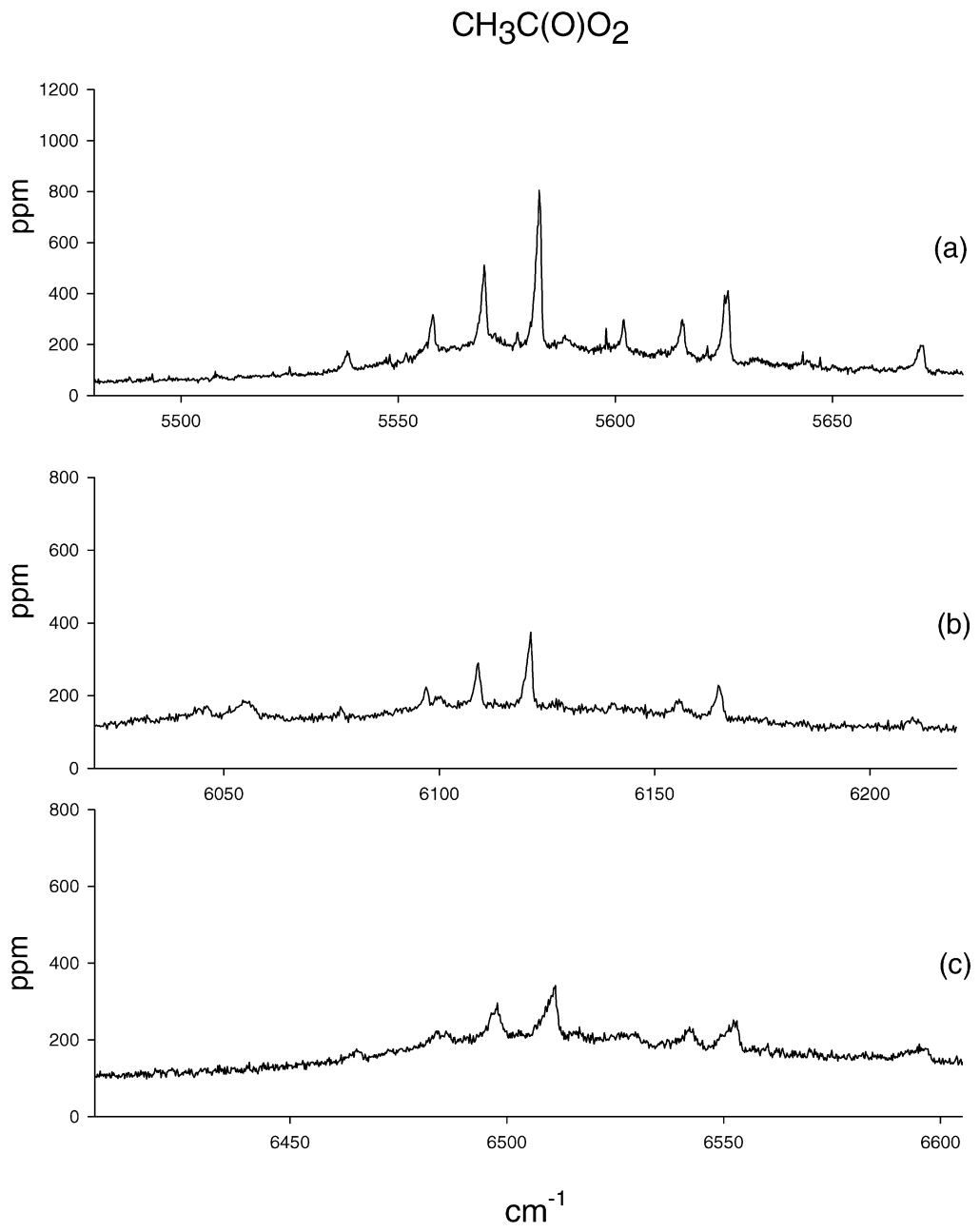

Figure 6. Experimental CRDS spectra of $CH_3C(O)O_2$: (a) Origin, (b) COO bend, (c) OO stretch. The weak absorption band at ≈ 6050 cm^{-1} is attributed to the CCOO backbone vibration in the $\tilde{A}$ state (see Table 6.)

TABLE 6: Calculated $\tilde{A}$ State UHF/6-31+G(d) Scaled Frequencies for the A′ Symmetry Modes that Have Terminal Oxygen Involved into Vibrational Motion[a]

	$\tilde{A}$	expt	mode	symmetry
	472	473(1)	CCOO backbone	A′
trans-$CH_3C(O)O_2$	546	539(1)	COO bend	A′
	1036	929(1)	OO stretch	A′
	397	473(1)	CCOO backbone	A′
cis-$CH_3C(O)O_2$	847	539(1)	COO bend	A′
	1052	929(1)	OO stretch	A′

[a] The unpaired electron is localized on terminal oxygen, and therefore, listed modes are expected to be the most active ones. As was mentioned in the text, only transitions to the A′ symmetry modes in the $\tilde{A}$ state are allowed from the vibrationless level in the $\tilde{X}$ state.

3.3. Absorption Cross Section Estimation. Given the spectroscopic assignment, the absorption cross section for the acetyl peroxy $\tilde{A}^2A'-\tilde{X}^2A''$ transition can be estimated if one can calibrate the initial concentration of acetyl peroxy radical. Equal amounts of acetyl peroxy radicals and HCl molecules are formed under our experimental conditions because of the very rapid reactions 2 and 3. In addition to spectra assigned to acetyl peroxy, we have observed sharp lines which remain after background subtraction and, therefore, are photolytically produced. Several such lines are shown in the insert to Figure 4. Assisted by the HITRAN[26] database, we have assigned those lines to the first vibrational overtone of HCl and used them for frequency and absorption intensity calibration because the line positions and absorption cross sections for HCl overtone lines are well established.

Using the known integrated absorption cross sections and the ringdown absorption signal, one can estimate the concentration of HCl as follows. As an example, the $H^{37}Cl$ P(6) line shown on the insert to Figure 4 has an integrated absorption cross section of $I = 1.2 \times 10^{-21}$ cm/mol from HITRAN and a

measured peak absorption, $S^p_{HCl} = 20$ ppm. According to the Beer−Lambert law

$$S^p_{HCl} = \sigma^p_{HCl}[HCl]L \quad (4)$$

where L is the sample path length of 13 cm. The peak absorption cross section, σ^p_{HCl}, can be related to the integrated absorption cross section I

$$\sigma^p_{HCl} = \alpha \cdot \frac{I}{\Delta\nu} \quad (5)$$

The numerical coefficient α is taken to be a unity (0.94 in case of Gaussian line shape), because the experimental line shape is Voight because of a convolution of instrumental, Doppler, and collisional effects. Under our experimental conditions the laser bandwidth is the dominant contribution. The HCl molecular line width (0.03 cm^{-1}) is significantly smaller than our laser line width (0.3 cm^{-1}) and eq 4 might not be generally valid. However, in the case of small molecular absorption signals, ringdown spectroscopy can still be used as a quantitative tool[35] with ringdown molecular absorption still being related to the concentration of absorbing species using Beer−Lambert law. Combining eq 4 and 5 one can calculate the [HCl] concentration

$$[HCl] = \frac{S^p_{HCl}\Delta\nu}{LI} = 3.8 \times 10^{14}\ cm^{-3} \quad (6)$$

Concentration measurements using several observed HCl lines resulted in an averaged [HCl] concentration of $(6\pm3) \times 10^{14}$ mol/cm^3, which is consistent with predictions from our kinetic model (see Figure 2). With the acetyl peroxy origin band peak absorption of $S^p_{CH_3C(O)O_2} = 805$ ppm, the sample path length of $L = 13$ cm and $[HCl] = [CH_3C(O)O_2]_0$ the peak absorption cross section, $\sigma^p_{CH_3C(O)O_2}$ is given by

$$\sigma^p_{CH_3C(O)O_2} = \frac{S^p_{CH_3C(O)O_2}}{L[HCl]} = (1 \pm 0.5) \times 10^{-19}\ cm^2 \quad (7)$$

This cross section is somewhat bigger but comparable to that of methyl peroxy[20] $\sigma^p_{CH_3O_2} = 0.3 \times 10^{-19}$ cm^2. It should be noted that we consider the value for both radicals as empirical cross sections under our ambient cell conditions and with our laser line width. It represents total absorption of many closely spaced, partially overlapping individual rotational lines in the Q branch convoluted with our laser line width.

4. Conclusions

Cavity ringdown spectroscopy has been successfully implemented to study an important member of the peroxy radical family, the acetyl peroxy radical. Extensive arguments are presented that the observed ringdown spectra are the $\tilde{A}^2A'-\tilde{X}^2A''$ electronic transitions of the $CH_3C(O)O_2$ and $CD_3C(O)O_2$ radicals. Ab initio calculations have been carried out to assign spectral carrier and analyze observed spectroscopic features such as vibrational hot bands, $\tilde{A}$ state fundamental vibrations, and rotational contours. It is most probable that the observed $CH_3C(O)O_2$ origin band at 5582.5(5) cm^{-1} and $\tilde{A}$ state vibrational fundamentals correspond to the trans acetyl peroxy conformer. However, high-resolution studies are necessary to confirm our conformer assignment.

It was demonstrated that the newly proposed source of chlorine atoms, $(COCl)_2$, can be efficiently used to produce peroxy radicals under ambient cell conditions. A byproduct of the proposed production scheme, HCl, has been used to calibrate acetyl peroxy radical concentration and hence to derive an empirical absorption cross section.

Acknowledgment. The authors gratefully acknowledge Vadim L. Stakhursky for upgrading data acquisition software, the Ohio Supercomputer Center for the grant of computational time and support of this work by the National Science Foundation via the Environmental Molecular Science Institute, Grant CHE-0089147, and via Grant CHE-0211281.

References and Notes

(1) Tyndall, G. S.; Cox, R. A.; Granier, C.; Lesclaux, R.; Moortgat, G. K.; Pilling, M. J.; Ravishankara, A. R.; Wallington, T. J. *J. Geophys. Res.* [*Atmos.*] **2001**, *106*.

(2) Tyndall, G. S.; Staffelbach, T. A.; Orlando, J. J.; Calvert, J. G. *Int. J. Chem. Kinet*. **1995**, *27*, 1009.

(3) Atkinson, R.; Lloyd, A. C. *J. Phys. Chem. Ref. Data* **1984**, *13*, 315.

(4) Wallington, T. J.; Nielsen, O. J. In *Peroxyl Radicals*; John Wiley and Sons: New York, 1997; Chapter Peroxy Radicals and the Atmosphere, p 69.

(5) Frost, G. J.; Ellison, G. B.; Vaida, V. *J. Phys. Chem. A* **1999**, *103*, 10169.

(6) Tomas, A.; Villenave, E.; Lesclaux, R. *J. Phys. Chem. A* **2001**, *105*, 3505.

(7) Crawford, M. A.; Wallington, T. J.; Szente, J. J.; Maricq, M. M. *J. Phys. Chem. A* **1999**, *103*, 365.

(8) Maricq, M. M.; Szente, J. J. *J. Phys. Chem*. **1996**, *100*, 4507.

(9) Roehl, C. M.; Bauer, D.; Moortgat, G. K. *J. Phys. Chem* **1996**, *100*, 4038.

(10) Grosjean, E.; Grosjean, D.; Fraser, M. P.; Cass, G. R. *Environ. Sci. Technol*. **1996**, *30*, 1731.

(11) Altshuller, A. P. *JAPCA J. Air Waste Manage*. **1978**, *28*, 594.

(12) Cape, J. N. *Environ. Pollut.* **2003**, *122*, 145.

(13) Edney, E. O.; Spence, J. W.; Hanst, P. L. *JAPCA J. Air Waste Manage*. **1979**, *29*, 741.

(14) Beine, H. J.; Jaffe, D. A.; Herring, J. A.; Kelley, J. A.; Krognes, T.; Stordal, F. *J. Atmos. Chem*. **1997**, *27*, 127.

(15) Lightfoot, P. D.; Cox, R. A.; Crowley, J. N.; Destriau, M.; Hayman, G. D.; Jenkin, M. E.; Moortgat, G. K.; Zabel, F. *Atmos. Environ. A-Gen*. **1992**, *26*.

(16) Wallington, T. J.; Dagaut, P.; Kurylo, M. J. *Chem. Rev*. **1992**, *92*, 667.

(17) Hunziker, H. E.; Wendt, H. R. *J. Chem. Phys*. **1976**, *64*, 3488.

(18) Bulatov, V. P.; Matyagin, Y. V.; Sarkisov, O. M.; Sviridenkov, E. A. *Khim. Fiz*. **1991**, *10*, 311.

(19) Fink, E. H.; Ramsay, D. A. *J. Mol. Spectrosc*. **1997**, *185*, 304.

(20) Pushkarsky, M. B.; Zalyubovsky, S. J.; Miller, T. A. *J. Chem. Phys*. **2000**, *112*, 10695.

(21) Schere, J. J.; Paul, J. B.; O'Keefe, A.; Saykally, R. J. *Chem. Rev*. **1997**, *97*, 25.

(22) Scherer, J. J.; Paul, J. B.; Collier, C. P.; O'Keefe, A.; Rakestraw, D. J.; Saykally, R. J. *Spectroscopy* **1996**, *11*, 46.

(23) Zalyubovsky, S. J.; Wang, D.; Miller, T. A. *Chem. Phys. Lett*. **2001**, *335*, 298.

(24) Atkinson, D. B.; Spillman, J. L. *J. Phys. Chem. A* **2002**, *106*, 8891.

(25) Berden, G.; Peeters, R.; Meijer, G. *Int. Rev. Phys. Chem*. **2000**, *19*, 565.

(26) Rothman, L. S.; Rinsland, C. P.; Goldman, A.; Massie, S. T.; Edwards, D. P.; Flaud, J. M.; Perrin, A.; Camy-Peyret, C.; Dana, V.; Mandin, J. Y.; Schroedera, J.; McCann, A.; Gamache, R. R.; Wattson, R. B.; Yoshino, K.; Chance, K. V.; Jucka, K. W.; Brown, L. R.; Nemtchinov, V.; Varanasi, P.; *HITRAN Molecular Spectroscopy Database and HITRAN Atmospheric Workstation*; Harvard Center for Astrophysics, 1996.

(27) Baklanov, A. V.; Krasnoperov, L. V. *J. Phys. Chem. A* **2001**, *105*, 97.

(28) Ahmed, M.; Blunt, D.; Chen, D.; Suits, A. G. *J. Phys. Chem*. **1997**, *106*, 7617.

(29) Bartel, M.; Hoyermann, K.; Lange, U. *Ber. Bunsen-Ges. Phys. Chem*. **1989**, *93*, 423.

(30) Lee, J.; Chen, C.-J.; Bozzelli, J. W. *J. Phys. Chem. A* **2002**, *106*, 7155.

(31) Martinez, R. D.; Buitrago, A. A.; Howell, N. W.; Hearn, C. H.; Joens, J. A. *Atmos. Envir*. **1992**, *26*,.

(32) Francisco, J. S.; Williams, I. H. *J. Chem. Phys*. **1988**, *92*, 5347.

(33) Benassi, R.; Taddei, F. *J. Mol. Struct.* **1993**, *303*, 83.

(34) Foresman, J. B.; Frisch, A. *Exploring Chemistry with Electronic Structure Methods: A Guide to Using Gaussian*, 2 ed.; Gaussian Inc.: Pittsburgh, 1998; pp 141−161.

(35) Zalicki, P.; Zare, R. N. *J. Chem. Phys.* **1995**, *102*, 2708.

(36) Tyndall, G. S.; Orlando, J. J.; Kegley-Owen, C. S.; Wallington, T. J.; Hurley, M. D. *Int. J. Chem. Kinet*. **1999**, *31*, 776.

(37) Adachi, H.; Basco, N.; James, D. G. L. *Chem. Phys. Lett*. **1978**, *59*, 502.

(38) Atkinson, R.; Baulch, D. L.; Cox, R. A.; Hampson, R. F.; Kerr, J. A.; Rossi, M. J.; Troe, J. *J. Phys. Chem. Ref. Data* **1997**, *26*, 521.

(39) DeMore, W. B.; Sandler, S. P.; Golden, D. M.; Hampson, R. F.; Kurylo, M. J.; Howard, C. J.; Ravishankara, A. R.; Kolb, C. E.; Molina, M. J. Technical Report 97-4; Jet Propulsion Laboratory, 1977.

(40) Maricq, M. M.; Ball, J. C.; Straccia, A. M.; Szente, J. J. *Int. J. Chem. Kinet*. **1997**, *29*, 421.

(41) Zalyubovsky, S. J.; Pushkarsky, M. B.; Miller, T. A. unpublished.

(42) Stakhursky, V. L. http://molspect.mps.ohio-state.edu/goes/specview.html.